THE JOURNAL OF PHYSICAL CHEMISTRY C

Caltech Library

Subscriber access provided by Caltech Library

C: Surfaces, Interfaces, Porous Materials, and Catalysis

Exploring the Nature of the Energy Barriers on the Mechanism of the Zirconocene-Catalyzed Ethylene Polymerization: A Quantitative Study from Reaction Force Analysis

Daniela E. Ortega, Ricardo A. Matute, and Alejandro Toro-Labbé

J. Phys. Chem. C, **Just Accepted Manuscript** • DOI: 10.1021/acs.jpcc.9b11615 • Publication Date (Web): 30 Mar 2020

Exploring the Nature of the Energy Barriers on the Mechanism of the Zirconocene-Catalyzed Ethylene Polymerization: A Quantitative Study from Reaction Force Analysis

Daniela E. Ortega,*,† Ricardo A. Matute, †,£ and Alejandro Toro-Labbé*,§

†Centro Integrativo de Biología y Química Aplicada (CIBQA), Universidad Bernardo OHiggins, Santiago 8370854, Chile.

£Division of Chemistry and Chemical Engineering, California Institute of Technology, Pasadena, California 91125, USA.

§Laboratorio de Química Teórica Computacional (QTC), Facultad de Química y Farmacia, Pontificia Universidad Católica de Chile, Casilla 306, Santiago-22, Chile.

ABSTRACT: Ethylene polymerization mediated by methyl-bis(cyclopentadienyl)-zirconium or zirconocene catalyst, $[ZrCp_2CH_3]^+$ is one of the most popular catalytic reaction for polyethylene production. Rationalizing the major effects that control the polymer growth result a challenge for computational studies. Through quantum chemical calculations, we characterized the zirconocene ethylene polymerization reaction mechanism; the chain initiation (**I**; first ethylene insertion) $[ZrCp_2CH_2CH_2CH_3]^+$, chain propagation (**P**; from second ($\mathbf{P_1}$) to ninth ($\mathbf{P_9}$) ethylene insertion) $[ZrCp_2(CH_2)_{20}CH_3]^+$ and chain termination processes (**T**; β-hydrogen elimination from $\mathbf{P_5}$ or $\mathbf{P_9}$) $[ZrHCp_2(H_2C{=}CH(CH_2)_{18}CH_3]^+$ are analyzed through potential energy surface (PES) and the reaction force analysis (RFA). The RFA approach involves pulling out the portion of an activation barrier that corresponds to distorting reactants into the geometries they adopt in a transition state structure until it reaches the structural relaxation toward the equilibrium geometry of the product. Because the interactions between the zirconocene and the ethylene molecule are influenced by a combination of several kinds of steric and electronic effects, it is indispensable to understand these interactions in order to rationalize and predict in a quantitative manner the reaction barrier heights and the concomitant polymer growth. In the present work, we employ a simple procedure within the framework of the RFA and the density functional steric energy decomposition analysis (EDA) approach to quantitatively separate the different types of interactions; steric (ΔE_s), electrostatic (ΔE_e), and quantum (ΔE_q) effects in order to predict the impacts of each factor on the course of the polymerization process as well as for the polymer control and design.

INTRODUCTION

Polyethylene (PE) is the most common plastic representing about 36% in the world, with an annual production of approximately 80 million metric tons.[1] The large-scale production of PE is closely linked to the development of coordination compounds, characterized by their high activity and low cost, although several catalytic systems for obtaining this polymer are known, those of the Ziegler-Natta[2-4] type have become the catalysts with the highest profitability in the industry. Ziegler-Natta catalysts have been widely developed in the last 50 years, which are efficient and selective compounds for many kinds of ethylene polymerization process[5] being the focus of intensive theoretical and experimental investigations over the last several years.[6-11] Today, PE produced with the help of these catalysts has become the largest plastic material together with polypropylene.[12]

Metallocene compounds show only one type of active site, in contrast to Ziegler-Natta systems producing polyethylene with narrow molecular weight distribution. Those typically used in the polymerization of ethylene, consist of transition metals of IVB group (Ti, Zr, and Hf), generally attached to aromatic rings of the Cyclopentadienyl type. The active species in the reaction is the metallocenic cation, which is generated by the action of methylaluminoxane (MAO), which has the function of activating the zirconocene catalyst by the abstraction of a chlorine atom generating a cationic catalyst that is stabilized by the anion of the MAO.[13] Specifically, the zirconocene/MAO catalyst system has proven to be 10 to 100 times more active than the classic Ziegler-Natta catalyst[14] with high catalytic efficiency for the polyethylene production of low molecular weight.[7,15] Experimentally was found that the performance of MAO is not strongly dependent on the catalytic activity for the zirconocene ethylene polymerization catalysis during the chain initiation, propagation, and termination steps.[17] The ethylene polymerization of zirconocene catalysts has paved the way for the design of new materials in the polymer industry is the focus on the increasing performance of standard plastics.[16]

In this paper, we have focused on the study of the ethylene polymerization process catalyzed by zirconocene, according to Scheme 1, without considering the co-catalyst or the solvent effects because it is not an issue of interest in this work. Our focus is the understanding of the reaction mechanism in terms of their reaction domain effects along with the zirconocene polymerization catalysis, which will be of significant interest, especially to industry. From quantum mechanics, it is

possible to study different thermodynamic models to estimate free energy changes in gas phase or solution (Figure S1), which have been applied in the computation of kinetic and thermodynamic properties such as rate constants. In thermodynamic cycle calculations, the intrinsic free energy corresponds to the change in Gibbs free energy of the system in the gas and solution phase using the following expression:

$$\Delta G^{\ddagger} = \Delta E^{\ddagger} + \Delta G_{RR\text{-}QHO} + \Delta G_{solv}. \quad (1)$$

The first term comes from activation enthalpy ($\Delta H^{\ddagger}$), which is analogous to the activation electronic energy quantity in the gas phase ($\Delta E^{\ddagger} = \Delta H^{\ddagger} + RT$) compute on optimized geometries, while the last two terms correspond to the thermal contributions of the solution phase where the Gibbs free energy is calculated through the partition function derived from the ideal gas rigid-rotor harmonic oscillator approximation. These energies can be obtained directly from electronic structure calculations. In general, the intrinsic Gibbs free energy shows a diverse data set that will provide a rigorous treatment toward a more specific and reliable alternative to calculate the thermodynamic and kinetic of a chemical process. We will study the thermodynamic cycle in the gas phase, where although the solvation induced significant changes in the structure and in the catalysis of a chemical system, which is another alternative of a possible direction for future work.

The initiation (**I**), propagation (**P**), and β-hydrogen elimination as chain termination (**T**) steps were studied by DFT calculations according to Scheme 1. The generic mechanism, better known as Cosse-Arlman mechanism[18-19] of ethylene insertion reaction, involves the coordination of a unit of ethylene (not modeled here) to form a π-complex, followed by ethylene insertion between the Zr-CH_3 bond, this process has been identified as chain initiation (**I**). Chain propagation process (**P**) is initiated by olefin uptake to give place to the subsequent insertions, where nine ethylene insertions were studied for this step. The transfer of β-hydrogen in the polymer to the Zr atom through an agostic interaction was analyzed in termination of the chain (**T**) because it is the kinetically preferred chain termination on the zirconocene catalyst.[7] We are mainly interested in emphasizing on the polymer chain propagation. In any catalytic coordination polymerization process of ethylene, there are several parameters that account for the effectiveness of this process, such as the molecular weight, the polydispersity index, or degree of polymerization and catalytic activity.[20] The knowledge of these factors is essential for the understanding of the evolution of the new polymer formed in time scale as well as for the design and control of the polymer.

The study of accurate methods to predict reaction mechanisms and the energetic of chemical reactions is an area of active research. Quantitative Structure-Activity Relationship (QSAR) studies, machine learning as well as DFT methods have been carried out as plausible methods for approximating results for complex polymerization reactions, yielding insight into the catalytic mechanism of olefin polymerization catalysts.[21-23] Besides, rationalizing the major effects that control polymer growth has become a challenge for computational studies. The steric and electronic effects on the catalyst are also expected to contribute to the control of the formed polymer that has an impact on the course of the polymerization process. Any chemical reaction could be described in terms of steric and electronic effects through the potential energy E(ξ) of the total system along the intrinsic reaction coordinate (IRC = ξ). [24-25] Based upon the classical expression for the force, the negative gradient of the E(ξ) along a suitable reaction coordinate gives a force in the direction opposite to that of increasing energy; and it has been named by Toro-Labbé as the reaction force analysis (RFA), F(ξ).[26] RFA shows a minimum and a maximum at the inflection points of E(ξ) different regions

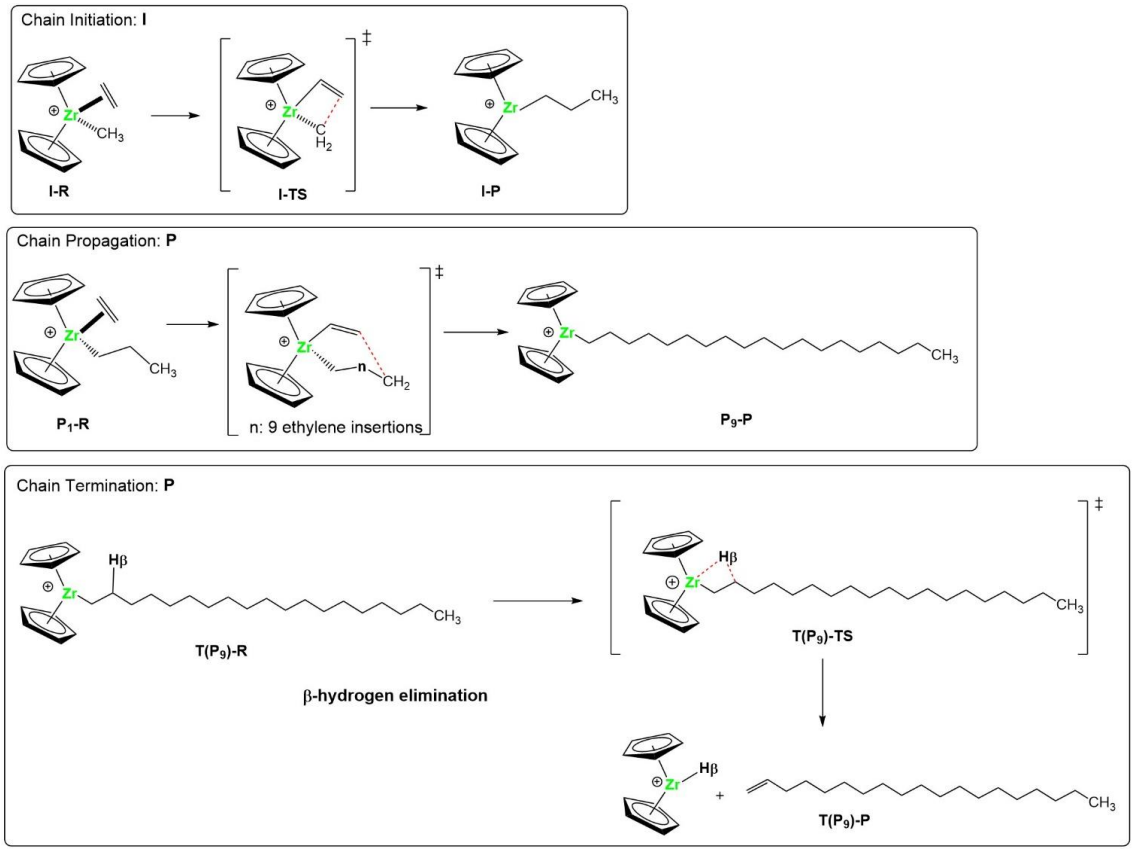

Scheme 1. Chain initiation (**I**), propagation (**P**) and termination (**T**) steps for bis-cyclopentadienyl zirconium catalyst.

along the reaction coordinate can be defined[27] as shown in Scheme 2a. To each step of the reaction within a given reaction region, the energy involved along the reaction coordinate can be rationalized through reaction works (W_i),[26] which have opened a way for rationalizing the catalytic properties of different compounds and for predicting their catalytic activity[28] providing an alternative approach to characterize the distortion independently of the molecularity of a reaction. RFA is a partition that is a natural consequence of the fragmentation of the reaction coordinate in regions. This approach involves pulling out the portion of an activation barrier that corresponds to distorting reactants into the geometries they adopt in a transition state structure until it reaches the structural relaxation toward the equilibrium geometry of the product. This decomposition scheme has a certain analogy with the distortion and interaction components that have been described separately by Morokuma, Bickelhaupt and Houk (called reactant deformation,[29] activation-strain model[30] or distortion-interaction, [31] respectively).

The potential energy profiles along the reaction coordinate have been used to discuss the mechanisms of ethylene polymerization on zirconocene active species, which allow a simple interpretation of the reaction mechanism.[10] However, through the reaction force analysis [32] profiles we can simplify the complicated mechanistic details that cannot be identified by the potential energy profile quantifying the energetic cost of each process that takes place during a reaction mechanism through the reaction works, where the thermodynamic (ΔE°) and kinetic ($\Delta E^{\ddagger}$) energy barriers can be calculated characterizing their physical nature in terms of the reaction works (see Scheme 2a). Based on previous studies, the reactant and product regions are dominated by steric rearrangements (bond lengthening, rotation, angle changes, etc.), whereas the transition state region is characterized by an intensive electronic activity through a collection of chemical events (bond strengthening/formation and bond weakening/breaking). Although the predominance of those phenomena is not exclusively within each reaction region. It is for that reason that the quantitative understanding of the dominant factors controlling the reaction barrier heights remains controversial. It is well known that the ethylene polymerization process control is based on mainly steric interactions between the catalyst and the ethylene substrate that is being inserted over the metal, which significantly slows down the reaction due to steric hindrance (Scheme 2b). In addition, a sensible explanation for the chain growth control and the catalytic activity could be based on favored orbital interactions (stereoelectronic effects) between the catalyst and the ethylene molecule (Scheme 2b). Therefore, a thorough understanding of how the different effects contribute to catalytic activity is essential for the development of similar catalysts for PE production.

We present a systematic computational study to quantitatively analyze the nature of the contributions that impact on the ethylene polymerization reaction barriers using the density functional steric energy decomposition analysis (EDA) method developed by Liu, [33] which has been widely applied to a variety of chemical compounds to study conformational changes,[34]the physical differences between branched and linear alkanes,[35] stereoelectronic effects[36], etc.[37] The computed barriers were dissected in terms of steric (ΔE_s), electrostatic (ΔE_e) and quantum (ΔE_q) effects. This approach quantifies the steric effect from DFT, assuming that the total energy comes from those three contributions. The steric component is defined as kinetic in nature by the Weizsäcker kinetic energy.[38] More importantly, it is easy to compute with any DFT method due to its unique dependence on the electron density and its gradient. This energy decomposition approach implemented within the theoretical framework of the RFA allows rationalizing the energetic contributions that impact the catalytic activity of the chain growth on zirconocene ethylene polymerization catalysis. Each reaction work (W_i) along the reaction coordinate, as well as the computed activation energy ($\Delta E\ddagger$), can be dissected into three contributions, called as steric (ΔE_s), electrostatic (ΔE_e) and quantum (ΔE_q). This will allow to reveal and understand the effects that originate the polymer growth in many kinds of catalytic systems active for PE production, which could be rationally predicted.

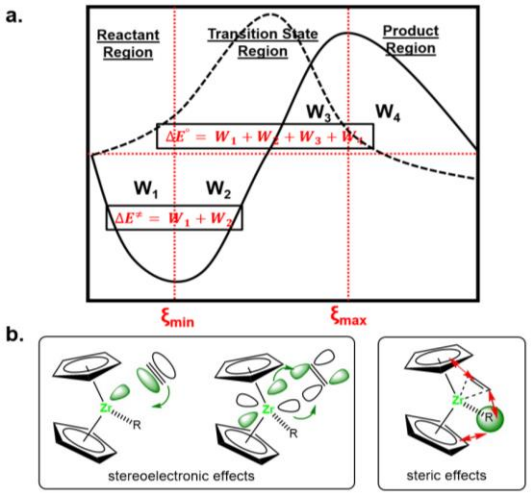

Scheme 2. (a) Typical profile of the potential energy (dashed line) and reaction force (solid line) for a 1-step reaction. {ξ_{min}, ξ_{max}} are the critical points localized between the reactant region and the transition state region; the second one is localized between the transition state and the products. The reaction works W_1-W_4 allow to characterize the physical nature of the activation $\Delta E^{\ddagger}$ and reaction ΔE° energies in terms of the prevalence either of steric {W_1,W_4} or electronic works {W_2,W_3}.[39] (b) Possible effects involved throughout the physical nature of the barriers in the mechanism of zirconocene ethylene polymerization catalysis.

METHODS

For each process, the reactants, transition states, and products geometries and energies were calculated using Gaussian 09 package [40] with the hybrid Meta-GGA density functional M06-2X.[41] The basis set used for non-metal atoms is 6-31+G(d,p),[42-45] Zr was described using the LANL2DZ pseudo-potential.[46] The characterization of the located stationary points was carried out by analytical frequency calculations, which were confirmed for all reactants and products with zero imaginary frequencies and for transition states with the first-order saddle points on the potential energy surface. The minimum energy path from the reactants to the product was calculated through the intrinsic reaction coordinate (IRC). [24-25] The profiles of $E(\xi)$ and $F(\xi)$ were obtained through single-point calculations on the previously optimized geometries of the supermolecule obtained from the IRC procedure.

Density functional steric EDA[33] was computed using Multiwfn 3.7 program[47]by single point calculations on the computed gas-phase IRC in order to dissect the activation energy in terms of the steric ($W_{i\text{-}s}$), electrostatic ($W_{i\text{-}e}$) and quantum ($W_{i\text{-}q}$) reaction works. This energy decomposition method does not qualitatively depend on the basis set or density functionals, [33-34] assuming that the energy difference of a molecule only comes from three independent effects:

$$\Delta E = \Delta E_s + \Delta E_e + \Delta E_q \quad (2)$$

Steric (ΔE_s), electrostatic (ΔE_e), and quantum (ΔE_q) effects. In DFT the energy difference is partitioned by the contributions of the non-interacting kinetic (ΔT_s), the electrostatic (ΔE_e) and the exchange-correlation (ΔE_{xc}) energy density functionals: [48]

$$\Delta E = \Delta T_s + \Delta E_e + \Delta E_{xc} \quad (3)$$

Where the electrostatic term includes the nuclear-electron attraction (ΔV_{ne}), classical electron-electron Coulomb repulsion (ΔJ) and nuclear-nuclear repulsion energies (ΔV_{nn}),

$$\Delta E_e = \Delta V_{ne} + \Delta J + \Delta V_{nn} \quad (4)$$

In analogy to the DFT energy partition, the density functional steric EDA also uses the electrostatic contribution; however, the steric contribution is their main stabilization effect. The steric contribution is expressed by the Weizsäcker kinetic energy: [38]

$$E_s \equiv T_W = {}^1\!/_8 \int \frac{|\nabla \rho(\boldsymbol{r})|^2}{\rho(\boldsymbol{r})} d\boldsymbol{r} \quad (5)$$

Which represents the spatial distribution of the electron density being a repulsive effect (negative) in nature because it relates to the occupied space and is extensive in size due to the notion that the bulkier it is the system larger the steric effect will be. In contrast with the wavefunction quantification where the steric effect is associated with the Pauli Exclusion Principle. While, the contribution from the quantum effect comes from the exchange-correlation interaction and the Pauli component in the kinetic energy ($E_{Pauli} \equiv T_S - T_W$):

$$E_q = E_{XC} + E_{Pauli} \quad (6)$$

Therefore, E_q is physically attributed as a quantum contribution due to the quantum nature of the above principle, which is associated to the repulsions between filled orbitals (the available space to each electron decreases), increasing the energy of the system.

The density functional steric EDA approach can be extended to concepts as Non-covalent interactions (NCI)[49] method. This method is based on the electron density and the reduced density gradients (RDG) characterizing an isosurface associated to the spatial area of the interaction, while the sign of the second eigenvalue of the density Hessian characterizes attractive or repulsive interactions playing a fundamental role determining qualitatively the inter and intramolecular non-covalent interactions by colors (red, strong repulsion; blue, strong attraction and green, weak interaction). The kinetic interpretation of RDG allows us to connect with the Weizsäcker kinetic energy, hence in this context, NCI plots can be interpreted as those regions where the steric effect decreases. Therefore, this method was used in this work to characterize the interactions between the zirconocene catalyst and the ethylene molecule. NCI surfaces also were generated by the Multiwfn 3.7 program.

Stereoelectronic interactions were determined using natural bond orbital (NBO) second-order perturbation theory[50] to quantify key interactions between the zirconocene catalyst and ethylene substrate.

All molecular structures with their corresponding energies are available in the Supporting Information (SI).

RESULTS AND DISCUSSION

In the following, we will discuss the energetic details of the polymerization process before applying the Density functional steric EDA analysis to characterize the polymer growth. The potential energy, reaction force profiles, and energetic results

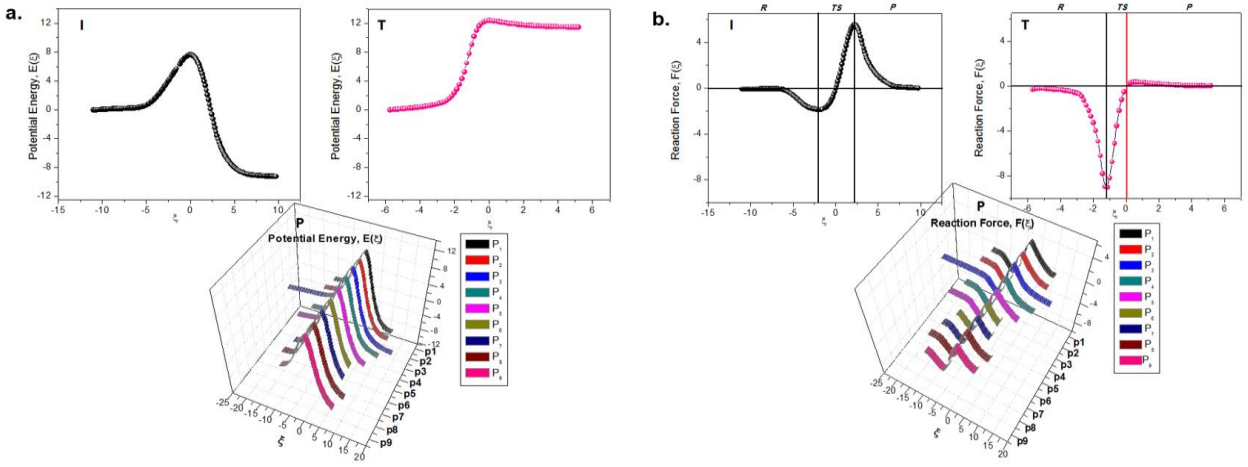

Figure 1. (a) Potential energy profiles for the initiation (**I**), propagation (**P**) and termination (**T**) process in kcal mol^{-1} vs. reaction coordinate for bis- cyclopentadienyl zirconium catalyst. (b) Reaction force profiles for the initiation (**I**), propagation (**P**) and termination (**T**) process in kcal mol^{-1} vs. reaction coordinate for bis- cyclopentadienyl zirconium catalyst.

of our DFT calculations are summarized in Figure 1 and Table 1, respectively.

The addition of an ethylene molecule to the zirconocene methyl cation proceeds in a barrierless fashion to give a π-complex (**I-R**; Figure 2) by a thermodynamically favored process with an associated energy cost of -27.40 kcal mol^{-1}. Also, it can be seen that the initiation process is kinetically (7.76 kcal mol^{-1}) and thermodynamically (-9.01 kcal mol^{-1}) favorable. The propagation reaction increases its activation energy progressively to a fifth insertion (**P$_5$**), where it subsequently decreases gradually until reaching equilibrium (**P$_9$**), with an average of 9.54 kcal mol^{-1}, corresponding to the activation energy for the propagation process. Surprisingly, the activation energy of the first insertion (initiation step) is much

Table 1. Activation barriers $\Delta E^{\ddagger}$, total reaction energies ΔE° and reaction work W_i (i=1,2,3 and 4) in terms of Density functional steric EDA for the ethylene polymerization process (**I**, **P** and **T**) for bis-cyclopentadienyl zirconium catalyst. **T(P$_9$)** and **T(P$_5$)** indicate the modeling of the termination step from **P$_9$** and **P$_5$** product, respectively. Energies are in kcal mol^{-1}.

Reaction Steps	$\Delta E^{\ddagger}$	ΔE°	W_i	ΔE_e	ΔE_s	ΔE_q
Activation	-	-27.40	-	-105.01	-103.94	181.55
I	7.76	-9.01	**W$_1$:** 5.73	0.40	-98.69	104.02
			W$_2$: 2.03	19.20	-62.98	45.81
			W$_3$: -6.87	13.08	-90.00	70.05
			W$_4$: -9.90	-32.97	-14.91	37.98
P$_1$	9.67	-8.74	**W$_1$:** 6.73	-9.62	-62.14	78.49
			W$_2$: 2.94	29.09	-55.91	29.76
			W$_3$: -5.26	18.86	-67.57	43.45
			W$_4$: -13.15	-49.04	30.89	5.00
P$_2$	9.85	-7.79	**W$_1$:** 6.85	-10.95	-69.81	87.61
			W$_2$: 3.00	32.85	-53.04	23.19
			W$_3$: -5.31	20.34	-64.26	38.61
			W$_4$: -12.33	-47.61	36.68	-1.40
P$_3$	10.16	-8.09	**W$_1$:** 7.39	-7.45	-45.93	60.77
			W$_2$: 2.77	28.88	-56.08	29.97
			W$_3$: -5.35	18.82	-67.65	43.48
			W$_4$: -12.90	-45.93	31.57	1.46
P$_4$	9.29	-7.91	**W$_1$:** 5.85	-6.80	-80.16	92.81
			W$_2$: 3.44	31.85	-59.66	31.25
			W$_3$: -5.09	15.75	-66.93	46.09
			W$_4$: -12.11	-42.74	35.88	-5.24
P$_5$	9.39	-7.95	**W$_1$:** 6.42	-3.58	-93.97	103.97
			W$_2$: 2.97	29.16	-53.19	27.00
			W$_3$: -5.06	9.34	-67.30	52.90
			W$_4$: -12.28	-37.86	45.10	-19.52
P$_6$	9.85	-7.58	**W$_1$:** 6.44	-9.68	-22.48	38.60
			W$_2$: 3.41	30.98	-61.34	33.77
			W$_3$: -5.06	16.05	-67.96	46.85
			W$_4$: -12.37	-43.43	38.88	-7.82
P$_7$	9.77	-7.52	**W$_1$:** 6.35	-8.46	-9.06	23.87
			W$_2$: 3.42	31.01	-60.77	33.18
			W$_3$: -5.07	15.95	-67.37	46.35
			W$_4$: -12.22	-43.20	39.40	-8.42
P$_8$	8.78	-8.82	**W$_1$:** 5.41	-6.23	-85.96	97.60
			W$_2$: 3.37	30.90	-63.46	35.93
			W$_3$: -5.08	16.02	-69.94	48.84
			W$_4$: -12.52	-42.31	24.93	4.86
P$_9$	9.07	-8.19	**W$_1$:** 5.55	-6.99	-83.54	96.08
			W$_2$: 3.52	31.38	-59.24	31.38
			W$_3$: -5.09	15.84	-65.64	44.71
			W$_4$: -12.17	-43.07	38.33	-7.43
T(P$_5$)	12.73	11.37	**W$_1$:** 12.44	-27.24	78.99	-39.31
			W$_2$: 0.29	18.46	-21.87	3.70
			W$_3$: -5.99	32.33	-38.79	0.47
			W$_4$: 4.63	-40.51	132.73	-87.59
T(P$_9$)	12.86	12.03	**W$_1$:** 12.61	-25.27	93.67	-55.79
			W$_2$: 0.25	17.46	-22.74	5.53
			W$_3$: -5.85	34.65	-39.84	-0.66
			W$_4$: 5.02	-41.20	129.75	-83.53

smaller than for the chain propagation, whereas the alkyl chain grows, the catalytic activity should increase. This can be argued for reasons of steric character since as the chain length increases, a greater distance from the metal center could favor the insertion of monomer and, therefore, the ethylene uptake for polymerization of the latter. However, in the initiation step, the ethylene complexation is much stronger than in the propagation. This difference is due to the lack of stabilizing agostic interactions in the **I-R** and **I-TS** structures (see Figure 2), which could be explained in terms of steric effects. The presence of an alkyl chain longer than methyl results in a smaller Cp-Zr-Cp angle, from 86° to 78° for the transition state structures in the **I** and **P** steps, respectively (Figure 2) and, consequently, a closer approach of the cyclopentadienyl ligands. However, the proximity between hydrogens in the forming chain of the catalyst during the propagation can be indicative of attractive dispersion stabilizations (**P** species in Figure 2) as well as in the γ-agostic products formed during the propagation step (**P_1-P**, **P_5-P,** and **P_9-P** in Figure 2). Therefore, compared with the γ-agostic products, the **I-P** cation is relatively more stable only by the lowest cyclopentadienyl ligand repulsions with the metallic center. Hence, the calculated reaction energy is ~1 kcal mol^{-1} higher in the propagation than in the initiation step.

Chain termination starts with β-agostic structure (**T(P_9)-R**, Figure 2) then takes place β-hydride elimination to the metal center. The chain termination is the rate-determining step

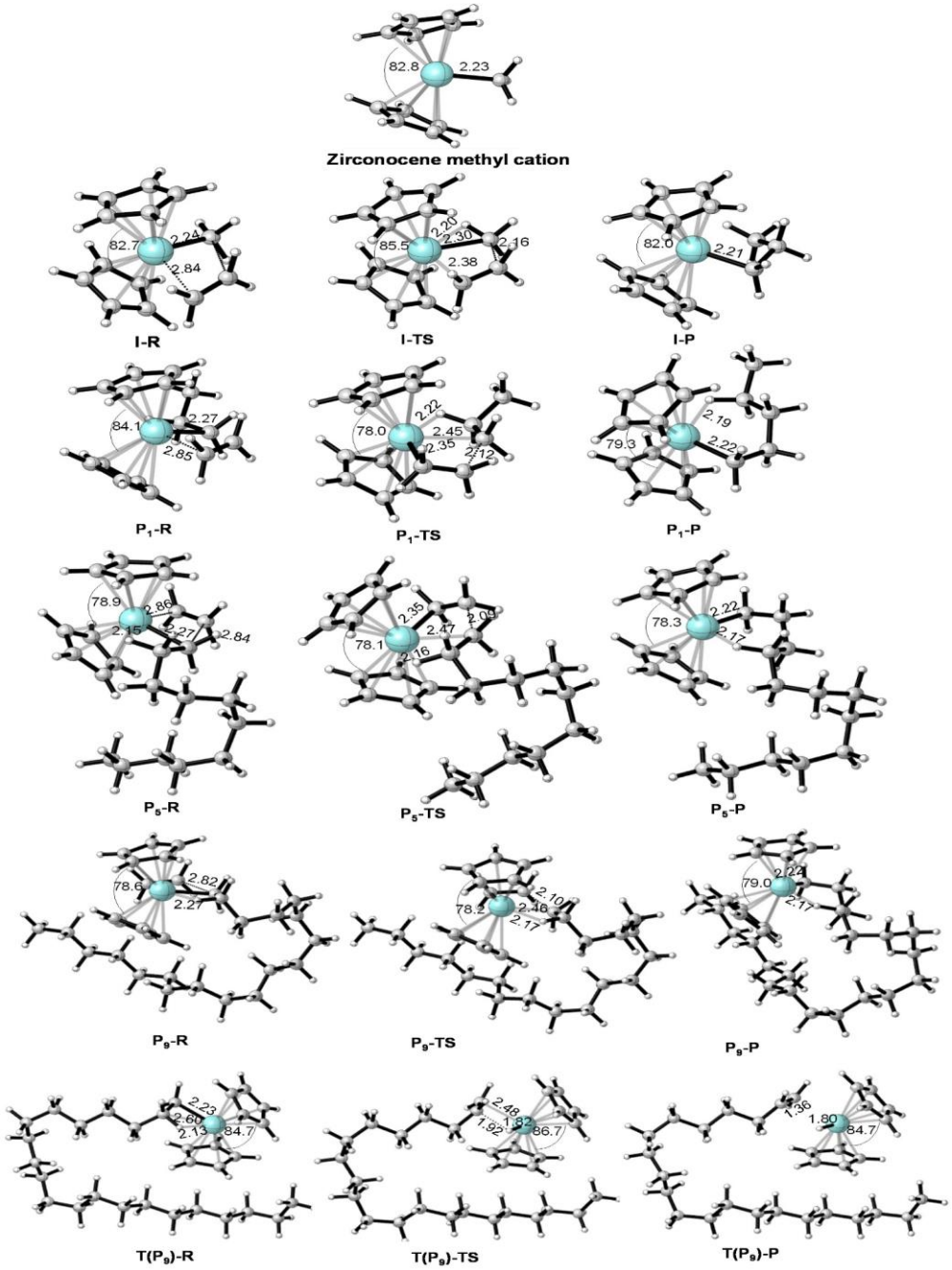

Figure 2. Geometries of the stationary points for the zirconocene methyl cation, chain Initiation (**I**), chain propagation (**P**) for one (**P_1**), five (**P_5**) and nine (**P_9**) ethylene insertions, chain termination (**T**). **R**, **TS** and **P** denote reactant, transition state and products.

reaching around 13 kcal mol^{-1}, where the transfer of H$_\beta$ to zirconium has found to be strongly endothermic. Note that β-hydride elimination calculated from five **T(P$_5$)** or nine **T(P$_9$)** ethylene molecules inserted are similarly unfavorable.

Chien[51] suggested estimation of the overall activation barrier using the following expression: $\Delta E^{\ddagger} = \frac{1}{2}\Delta E_I^{\ddagger} + \sum \Delta E_P^{\ddagger} - \frac{1}{2}\Delta E_T^{\ddagger}$ ~7 kcal mol^{-1}, which could be attributed to the polymerization process of this system (with five or nine insertions of ethylene). This is consistent with the experimental findings of Chien and coworkers,[52-53] which indicates that the activation energy for zirconocene ethylene polymerization reaction does not exceed 7.6 kcal mol^{-1}. Moreover, it is known that the molecular weight of the formed polymer is associated with the chain termination step, so a kinetic-favored termination reaction could be related to a high value of molecular weight. In this work, the molecular weight from **T(P$_9$)** and **T(P$_5$)** are 7603.4 g mol^{-1} and 4902.52 g mol^{-1}, respectively, which were computed from the degree of polymerization ($\overline{P_n}$) in terms of reaction rates given by the ratio between the overall rate of propagation (k_P), and the rate of chain termination reaction (k_T) reactions multiplied by the molecular weight of the repetitive unit (ethylene; 28 g mol^{-1}). However, the kinetic of the termination steps for long **T(P$_9$)** and short **T(P$_5$)** alkyl chain formations are very similar ($2{\cdot}10^3$ s^{-1} and $3{\cdot}10^3$ s^{-1}, respectively) indicating that the probability of forming a high molecular weight polymer will not be necessarily associated with its catalytic activity in the termination step (see also Figure S2). This clearly indicates the need to provide a chemically quantitative explanation about factors dictating the nature of the ethylene polymerization reaction barrier heights. We performed a density functional steric energy decomposition analysis within the framework of the RFA (Table 1).

First, using the reaction force analysis, the activation energy of each transition state along the ethylene polymerization reaction is decomposed into W_1 and W_2. Then, using the density functional steric EDA method, the reaction works are dissected into steric (ΔE_s), electrostatic (ΔE_e) and quantum (ΔE_q) effects (for more details, see computational methods section). To analyze how the zirconocene-ethylene interactions vary along the polymerization process, the computed energy terms concerning the reaction works are presented in Table 1. A few general conclusions about the activation barriers can be derived from the comparison of the reaction works W_1 and W_2 in each step of the ethylene polymerization process. Table 1 indicates that all reaction steps of the polymerization process are kinetically driven by W_1, energy mainly dominated by the change of quantum (ΔE_q) and steric effects (ΔE_s) along the **I**

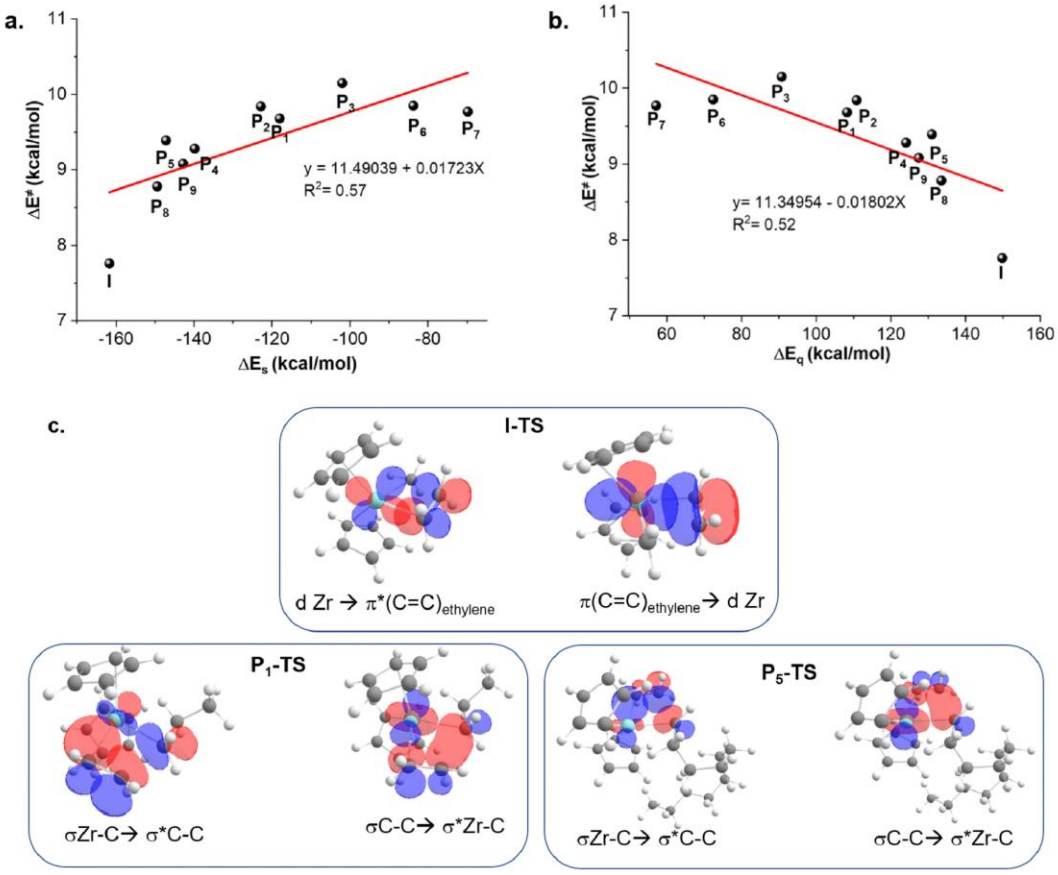

Figure 3. Correlations of the activation energy from the chain initiation to chain propagation of the ethylene polymerization reaction with; (a) the steric energy difference (ΔE_s) and with (b) the quantum energy difference (ΔE_q). (c) NBO overlap for the transition state structures associated to the chain initiation (**I-TS**) and propagation (**P$_1$-TS** and **P$_5$-TS**) ethylene polymerization reaction.

and **P** steps, with little contribution from the electrostatic effect, $\Delta E_e \approx$ 22 kcal mol^{-1} associated to the activation energy ($W_1 + W_2$), consequently does not correlate with the activation energy (R^2=0.005, Figure S3). While the contribution from quantum and steric effects found to be linearly proportional to the barrier heights with a moderate correlation coefficient R^2 of 0.57 (ΔE_s) and 0.52 (ΔE_q) as shown in Figure 3a and 3b. Although both correlation coefficients are not very high, there is a reverse trend between the data points for each geometry along the graphs 3a and 3b as a mirror image. The steric effect contributes to the height barrier negatively and the quantum effect does so positively (see ΔE_s and ΔE_q, respectively, in Table 1). Quantum effect shows a marked increase in energy when the non-bonded zirconium atom from the zirconocene catalyst and one of the carbon atoms from the monomer are forced to occupy the same space (Figure 3b) as shown for the chain initiation and for the propagation of longer chains as **P8** and **P9**, which at the same time have less steric hindrance (Figure 3a). This explains why these reactions are easily affected by lower barriers with respect to the earliest steps of propagation (see Table 1). It should not be forgotten that although ΔE_s and ΔE_q are repulsive in nature, ΔE_s is associated with the spatial volume of the system, while ΔE_q is associated with the distribution of the average volume available to each electron. Therefore, this indicates that the ethylene insertion barriers are associated to stereoelectronic nature. Indeed, stereoelectronic effects are simply associated with the spatial position of the molecular orbitals (Scheme 2b), a fact that has kinetic consequences. The steric effect presents a positive slope, indicating that there is an important steric hindrance associated to the orbital interactions. To understand why stereoelectronic effects promote the catalytic activity during the chain initiation and propagation steps, we performed NBO analysis using the second-order perturbation analysis of donor-acceptor interactions between the zirconocene catalyst and the ethylene molecule in the transition state structures (Figure 3c).

The NBO analysis revealed that the stabilization energies (E^2) associated with the orbital interaction between the occupied ethylene π orbital and the vacant zirconium d orbital (**I-TS**; π→d in Figure 3c) is the most important orbital interaction for the chain initiation step ($E^2_{(\pi\rightarrow d)}$ =64.55 kcal mol^{-1}, $E^2_{(d\rightarrow\pi)}$= 1.63 kcal mol^{-1}). This is a result of the zirconium as an electron-poor orbital (d^0) being a good σ-acceptor, which promotes the complexing of ethylene with zirconium. Furthermore, the net electron donation from the ethylene to zirconium would increase the electron density on the zirconium atom, which also supports the fact that there is not an agostic interaction in contrast to the chain propagation step. As discussed earlier, the chain propagation step presents a more advanced transition state structures showing Zr-C (with α-carbon of the ethylene molecule) and C-C (with β-carbon of the ethylene molecule) bond forming. This is associated with the shortening Zr-C bond in the transition state structures along the chain propagation (see Figure 2; **P1-TS**, **P5-TS,** and **P9-TS**) decreasing in the angle Cp-Zr-Cp strains in transition state structures, thus confirming the increase of the activation energy barriers. One interpretation of this result is that the π-complex is more stable than in the initiation step because the electron-donating σZr-C to σ*C-C enhances the back-donation electron density to the σ*C-C orbital of the monomer of ethylene ($E^2_{(\sigma Zr\text{-}C \rightarrow \sigma^*C\text{-}C)} \approx$ 42 kcal mol^{-1}, $E^2_{(\sigma C\text{-}C \rightarrow \sigma^*Zr\text{-}C)} \approx$ 18 kcal mol^{-1}). Another possible explanation is that the agostic interactions in the transition state can form a more stable complex to inhibit the latter's ability to catalyze the ethylene polymerization, therefore, since the chain length is limited by agostic interactions on the zirconocene ethylene polymerization catalysis, the chain propagation step result more difficult than the chain initiation.

On the other hand, we then employed the density functional steric EDA approach to study the nature of the remaining reaction works (W_2, W_3, and W_4) during the chain propagation, as shown in Figure 4. These results reveal how the steric and electronic properties in the course of the chain growth affect the different regions defined by the reaction force along the reaction coordinate. We found that different components become dominant in different reaction reactions. Within the transition state region, steric interactions control the reaction work W_2 (Figure 4a; R^2=0.62), whereas in the reaction work W_3 a more moderate correlation with the quantum effect (Figure 4b; R^2=0.56) was found as the controlling factor. Since W_3 is greater in magnitude ($|W_3|$) than W_2 in almost 2 kcal mol^{-1}, it is secure to argue that ΔE_q is the dominant factor within the TS region but compensated by the stabilizing contribution from the steric effect. These results are in agreement with the earlier discussed (Figure 3), the stereoelectronic effect is dominant within the TS region, and thus should increase as the chain increases in size.

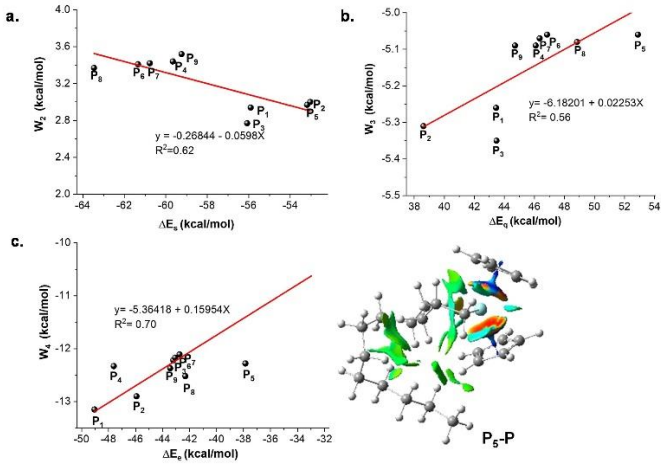

Figure 4. Correlations of the reaction work from the chain propagation of the ethylene polymerization reaction; (a) W_2 with the steric energy difference (ΔE_s), (b) W_3 with the quantum energy difference (ΔE_q) and (c) W_4 with the electrostatic (ΔE_e) energy differences. **P5-P** shows the NCI plot for this product structure in the chain propagation. The color spectrum ranges from; blue for strong attractions, green for weak interactions, and red for strong steric repulsions.

Surprisingly, the density functional steric EDA results indicate that within the product region, the reaction work W_4 is not very sensitive to the steric effects. We find a stronger linear correlation with the electrostatic energy difference (Figure 4c; R^2=0.70). The electrostatic effects are not particularly concerned with the interaction between the zirconocene catalyst and the ethylene substrate, because, within the product region, the alkene-metal complex is already formed. The stronger electrostatic interaction is attributed to the *γ*-agostic interactions in the products added to the attractive London dispersive non-covalent interactions. The NCI plot in Figure 4 shows weakly attractive interaction (the green slice) between the hydrogen atoms of the formed chain as well as the formed

chain with the cyclopentadienyl ligand of the zirconocene catalyst in the product, which is consistent with the greater electrostatic effects.

Finally, during the chain termination, the energy to overcome the retarding force is greater by about 6 kcal mol^{-1} with respect to W_1 associated with 98% of the activation barrier compared to the initiation and propagation steps about 70% of the activation energy corresponds to W_1. A narrow region associated with the transition state (Figure 1b; **T**) is further attributed with a high barrier for the chain termination and endothermic reaction energy becoming irreversible. This step requires the rupture of a C_β-H_β bond, which leads to a pronounced minimum of the reaction force (Figure 1b; **T**). After the minimum of the force, the effect that drives an increment of the force is due to the formation of a metal-hydrogen agostic interaction (Zr···H_β···C_β), which is a sign of an evident distinction of this profile for this process (Figure 1b; **T**). On the other hand, in contrast to the chain initiation and propagation steps, density functional steric EDA analysis indicated a substantially different selectivity control for the chain termination process. We find that for the chain termination, the steric effect is indeed the dominant factor, contributing positively to the activation barrier energy difference between the transition state and the reactant for shorter (from $\mathbf{P_5}$) or longer (from $\mathbf{P_9}$) chain formations (Figure 5a; ΔE_s). The larger steric contribution is a result of that the chain termination transition state must have a geometry that involves a coplanar arrangement for the zirconium atom with the C_β and H_β atoms of the propagating alkyl chain (Figure 5b; σZr-H_β→ π* C=C). Therefore, the chain termination becomes easier with the metallic center without π-complexed ethylene than for one with π-complexed ethylene. NCI plot in Figure 5b, for the transition state structure $\mathbf{T(P_9)}$, reveals that evidence on the reactive zone (red surface), although significantly stabilizing dispersion-like interactions (green surfaces), also takes place on the transition state.

Density functional steric EDA analysis on the reaction works W_2, W_3 and W_4 for the chain termination revealed that the transition state region governed by W_2 and W_3, the strong steric repulsion induced ($\Delta E_s \approx$ -62 kcal mol^{-1}) is compensated by electrostatic interactions ($\Delta E_e \approx$ 51 kcal mol^{-1}) with a little contribution of quantum effects ($\Delta E_q \approx$ 5 kcal mol^{-1}). This is in agreement with the stabilizing dispersion interactions appreciated in the NCI plot (Figure 5b). Regarding the product region, we found that in W_4 the electrostatic and quantum effects play a minor role in front of the high contribution from the steric effect ($\Delta E_s \approx$ 131 kcal mol^{-1}), which effectively override the other effects; thus indicating that the zirconocene catalyst is not active to a next ethylene insertion.

The dominant factors controlling the catalytic activity in zirconocene ethylene polymerization catalysis are summarized in Scheme 3. Although the steric effect is thought to be the majority in the course of the chain growth since as the chain length increases a greater distance from the metal center favoring the insertion of monomer occurs, the dominant factor on catalytic activity can be distinct. For the chain initiation and propagation steps, the stereoelectronic interactions are the most important factor that leads to the alkyl chain growth. In the chain termination, steric effects become the most important in the catalytic activity as well as in the chain length (molecular weight). Our computational study suggests that the energy decomposition analysis described by the reaction force may be applied to study the origin of the catalytic activity, reactivity, and selectivity of any other catalytic reaction.

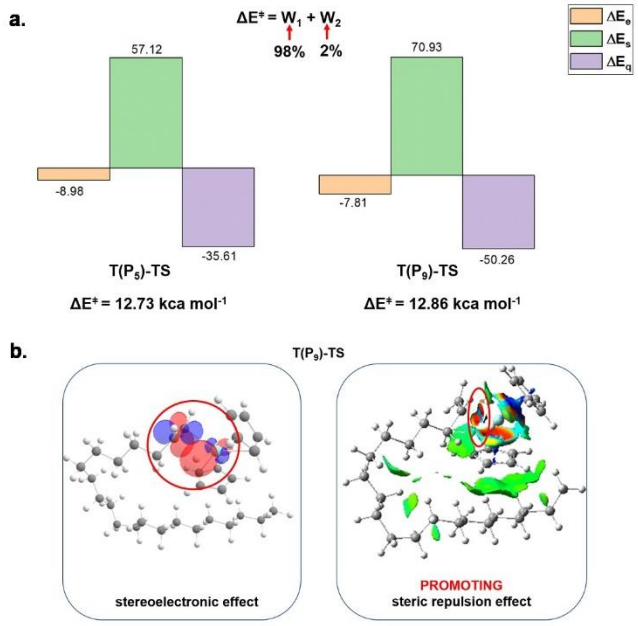

Figure 5. Origins of the activation energy barrier in the transition state associated with an earlier ($\mathbf{T(P_5)\text{-}TS}$) or later ($\mathbf{T(P_9)\text{-}TS}$) chain termination step. (a) The computed activation energy ($\Delta E^‡$) is calculated from the contributions of W_1 (98%) and W_2 (2%) in terms of each energy component (ΔE_e; orange, ΔE_s; green, ΔE_q; purple). All energies are in kcal mol^{-1}. (b) stereoelectronic (σZr-H_β→ π* C=C) and steric repulsion (red surface) effects on the reactive zone of the chain termination transition state.

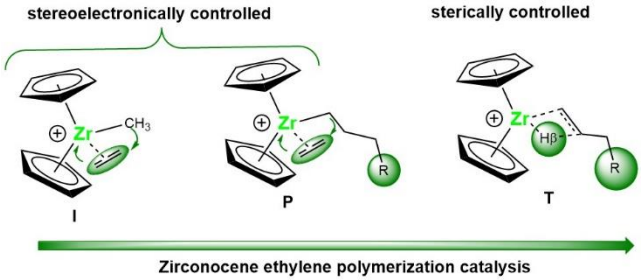

Scheme 3. Summary of the catalytic effects on the transition states along the zirconocene ethylene polymerization catalysis.

CONCLUSIONS

In this work, we presented a density functional steric energy decomposition approach within the framework of the RFA to rationalize the energetic contributions that impact the catalytic activity of the chain growth on zirconocene ethylene polymerization catalysis. The computed activation energy ($\Delta E^‡$) in terms of the reaction works (W_i) is quantitatively dissected into effects from electrostatics (ΔE_e) interactions, steric repulsions (ΔE_s), and quantum chemical interactions (ΔE_q) between the ethylene and the zirconocene in the transition states associated to the chain initiation, propagation and

termination steps for the polyethylene production. In addition, those effects are rationalized and characterized along the reaction regions involved in each step of the polymerization reaction. Therefore, the major factor controlling the catalytic activity and selectivity of the zirconocene ethylene polymerization catalysis and even with different catalytic reactions can be revealed in a practical and efficient fashion.

The results obtained in the present study are sufficient to allow some assumptions of the methods for controlling the catalytic activity of zirconocene catalyst for polyethylene production. The catalytic activity is dominated by W_1 being controlled for steric and quantum contributions, mainly due to the favorable stereoelectronic effects between the ethylene substrate and the zirconocene catalyst during the chain initiation and propagation. In the chain termination, stereoelectronic effects are diminished for the β-hydrogen elimination process, and the steric repulsions between the formed chain and the metallic center become more important on the catalytic activity. The use of this approach on the reaction works also allowed to know the dominant effects within the reactant, transition state, and product regions along the reaction coordinate. The reactant region is controlled by W_1, where stereoelectronic effects during the chain initiation and propagation, whereas in the termination step is controlled by steric repulsions. The transition state region involves W_2 and W_3, which revealed that along the whole course of the polymerization reaction, the steric repulsions are increased. Nonetheless, a stereoelectronic nature is present where the quantum effect is dominant but compensated by the stabilizing contribution from the steric effect and in the product region dominated by W_4, showed that the γ-agostic interactions and the dispersive interactions between the formed chain and the zirconocene catalyst increase the electrostatic effects during the chain growth. In addition, the product region for the chain termination is dictated by the diminished electrostatic effect that makes steric effects the dominant contribution to the β-agostic product.

We expect that the characterization of the catalytic activity described for the ethylene polymerization catalysis revealed in this study in terms of steric, electrostatic, and quantum effects within the RFA framework can provide insights to guide future design strategies for the catalytic polyethylene production as well as would allow to orient a reaction influencing specific regions of the reaction coordinate by means of the nature of substituent groups on the ligands, or effects granted by the nature of the substrate used in a given catalytic reaction.

ASSOCIATED CONTENT

Supporting Information. This material is available free of charge via the Internet at http://pubs.acs.org." All molecular structures with their corresponding energies are available (PDF).

AUTHOR INFORMATION

Corresponding Author

*E-mail: daniela.ortega@ubo.cl
*E-mail: atola@uc.cl

ORCID

Daniela E. Ortega: *0000-0002-0724-4206*
Ricardo A. Matute: *0000-0002-0644-3799*
Alejandro Toro-Labbé: *0000-0001-9906-2153*

Author Contributions

D.E.O. wrote the manuscript and performed all the calculations. Both R.A.M. and A.T.L. authors contributed to the final version of the manuscript. A.T.L. helped supervise the project.

Notes

The authors declare no competing financial interest.

ACKNOWLEDGMENT

D.E.O. acknowledges the financial support from the Postdoctoral FONDECYT Grant Nº 3190252. R.A.M and A.T.L. acknowledge the FONDECYT Grants Nº 1181260 and Nº 1181072.

REFERENCES

1. Geyer, R.; Jambeck, J. R.; Law, K. L., Production, Use, and Fate of All Plastics Ever Made. *Science Advances* **2017**, *3*, e1700782.
2. Ziegler, K.; Gellert, H.; Zosel, K.; Lehmkuhl, W.; Pfohl, W., Herstellung Von Aluminiumalkylen Und Dialkylaluminiumhydriden. *Angew. Chem.* **1955**, *67*, 424-424.
3. Ziegler, K.; Holzkamp, E.; Breil, H.; Martin, H., Das Mülheimer Normaldruck-Polyäthylen-Verfahren. *Angew. Chem.* **1955**, *67*, 541-547.
4. Natta, G., Polym Sci 1955, 16, 143. Wiley Online Library| CAS| Web of Science® Times Cited.
5. Böhm, L. L., The Ethylene Polymerization with Ziegler Catalysts: Fifty Years after the Discovery. *Angew. Chem. Int. Ed.* **2003**, *42*, 5010-5030.
6. Britovsek, G. J.; Gibson, V. C.; Wass, D. F., The Search for New-Generation Olefin Polymerization Catalysts: Life Beyond Metallocenes. *Angew. Chem. Int. Ed.* **1999**, *38*, 428-447.
7. Alt, H. G.; Köppl, A., Effect of the Nature of Metallocene Complexes of Group Iv Metals on Their Performance in Catalytic Ethylene and Propylene Polymerization. *Chem. Rev.* **2000**, *100*, 1205-1222.
8. Matsui, S.; Fujita, T., Fi Catalysts: Super Active New Ethylene Polymerization Catalysts. *Catal. Today* **2001**, *66*, 63-73.
9. Kaminsky, W., *Metalorganic Catalysts for Synthesis and Polymerization: Recent Results by Ziegler-Natta and Metallocene Investigations*; Springer Science & Business Media, 2012.
10. Martínez-Araya, J. I.; Quijada, R. l.; Toro-Labbé, A., The Mechanism of Ethylene Polymerization Reaction Catalyzed by Group Ivb Metallocenes. A Rational Analysis through the Use of Reaction Force. *The Journal of Physical Chemistry C* **2012**, *116*, 21318-21325.
11. Zhang, D.; Zi, G., N-Heterocyclic Carbene (Nhc) Complexes of Group 4 Transition Metals. *Chem. Soc. Rev.* **2015**, *44*, 1898-1921.
12. Malpass, D. B., Introduction to Industrial Polyethylene. *Wiley* **2010**, *Hoboken, NJ, USA*, 85-97.
13. Velthoen, M. E. Z.; Muñoz-Murillo, A.; Bouhmadi, A.; Cecius, M.; Diefenbach, S.; Weckhuysen, B. M., The Multifaceted Role of Methylaluminoxane in Metallocene-Based

Olefin Polymerization Catalysis. *Macromolecules* **2018**, *51*, 343-355.
14. Kashiwa, N., The Discovery and Progress of Mgcl2-Supported Ticl4 Catalysts. *J. Polym. Sci., Part A: Polym. Chem.* **2004**, *42*, 1-8.
15. Kaminsky, W., The Discovery of Metallocene Catalysts and Their Present State of the Art. *J. Polym. Sci., Part A: Polym. Chem.* **2004**, *42*, 3911-3921.
16. Maier, R.-D., Fortschritte Bei Metallocenprodukten. *Kunststoffe* **1999**, *89*, 120-132.
17. Song, F.; Hannant, M. D.; Cannon, R. D.; Bochmann, M., Zirconocene-Catalysed Propene Polymerisation: Kinetics, Mechanism, and the Role of the Anion. *Macromolecular Symposia* **2004**, *213*, 173-186.
18. Cossee, P., Ziegler-Natta Catalysis I. Mechanism of Polymerization of A-Olefins with Ziegler-Natta Catalysts. *J. Catal.* **1964**, *3*, 80-88.
19. Brintzinger, H. H.; Fischer, D.; Mülhaupt, R.; Rieger, B.; Waymouth, R. M., Stereospecific Olefin Polymerization with Chiral Metallocene Catalysts. *Angew Chem. Int. Ed.* **1995**, *34*, 1143-1170.
20. Kashiwa, N., The Discovery and Progress of Mgcl2-Supported Ticl4 Catalysts. *J. Polym. Sci., Part A: Polym. Chem.* **2004**, *42*, 1-8.
21. Yu, Y.; Cipullo, R.; Boisson, C., Alkynyl Ether Labeling: A Selective and Efficient Approach to Count Active Sites of Olefin Polymerization Catalysts. *ACS Catalysis* **2019**, *9*, 3098-3103.
22. Rizkin, B. A.; Hartman, R. L., Supervised Machine Learning for Prediction of Zirconocene-Catalyzed A-Olefin Polymerization. *Chem. Eng. Sci.* **2019**, *210*, 115224.
23. Bahri-Laleh, N.; Hanifpour, A.; Mirmohammadi, S. A.; Poater, A.; Nekoomanesh-Haghighi, M.; Talarico, G.; Cavallo, L., Computational Modeling of Heterogeneous Ziegler-Natta Catalysts for Olefins Polymerization. *Prog. Polym. Sci.* **2018**, *84*, 89-114.
24. Fukui, K., Formulation of the Reaction Coordinate. *J. Phys. Chem.* **1970**, *74*, 4161-4163.
25. Fukui, K., The Path of Chemical Reactions-the Irc Approach. *Acc. Chem. Res.* **1981**, *14*, 363-368.
26. Toro-Labbé, A., Characterization of Chemical Reactions from the Profiles of Energy, Chemical Potential, and Hardness. *J. Phys. Chem. A* **1999**, *103*, 4398-4403.
27. Politzer, P.; Toro-Labbé, A.; Gutiérrez-Oliva, S.; Herrera, B.; Jaque, P.; Concha, M. C.; Murray, J. S., The Reaction Force: Three Key Points Along an Intrinsic Reaction Coordinate. *J. Chem. Sci.* **2005**, *117*, 467-472.
28. Ortega, D. E.; Cortés-Arriagada, D.; Toro-Labbé, A., Mechanistic Details of Ethylene Polymerization Reaction Using Methallyl Nickel(Ii) Catalysts. *Phys. Chem. Chem. Phys.* **2018**, *20*, 22915-22925.
29. Nagase, S.; Morokuma, K., An Ab Initio Molecular Orbital Study of Organic Reactions. The Energy, Charge, and Spin Decomposition Analyses at the Transition State and Along the Reaction Pathway. *J. Am. Chem. Soc.* **1978**, *100*, 1666-1672.
30. Bickelhaupt, F. M., Understanding Reactivity with Kohn–Sham Molecular Orbital Theory: E2–Sn2 Mechanistic Spectrum and Other Concepts. *J. Comput. Chem.* **1999**, *20*, 114-128.
31. Ess, D. H.; Houk, K., Distortion/Interaction Energy Control of 1, 3-Dipolar Cycloaddition Reactivity. *J. Am. Chem. Soc.* **2007**, *129*, 10646-10647.
32. Toro-Labbé, A.; Gutiérrez-Oliva, S.; Murray, J.; Politzer, P., A New Perspective on Chemical and Physical Processes: The Reaction Force. *Mol. Phys.* **2007**, *105*, 2619-2625.
33. Liu, S., Steric Effect: A Quantitative Description from Density Functional Theory. *J. Chem. Phys.* **2007**, *126*, 244103.
34. Liu, S., Origin and Nature of Bond Rotation Barriers: A Unified View. *J. Phys. Chem. A* **2013**, *117*, 962-965.
35. Ess, D. H.; Liu, S.; De Proft, F., Density Functional Steric Analysis of Linear and Branched Alkanes. *J. Phys. Chem. A* **2010**, *114*, 12952-12957.
36. Huang, Y.; Zhong, A.-G.; Yang, Q.; Liu, S., Origin of Anomeric Effect: A Density Functional Steric Analysis. *J. Chem. Phys.* **2011**, *134*, 084103.
37. Fang, D.; Piquemal, J.-P.; Liu, S.; Cisneros, G. A., Dft-Steric-Based Energy Decomposition Analysis of Intermolecular Interactions. *Theor. Chem. Acc.* **2014**, *133*, 1484.
38. Weizsäcker, C. F. v., Zur Theorie Der Kernmassen. *Zeitschrift für Physik* **1935**, *96*, 431-458.
39. Ortega, D. E.; Gutiérrez-Oliva, S.; Tantillo, D. J.; Toro-Labbé, A., A Detailed Analysis of the Mechanism of a Carbocationic Triple Shift Rearrangement. *Phys. Chem. Chem. Phys.* **2015**, *17*, 9771-9779.
40. Gaussian09, R. A., 1, Mj Frisch, Gw Trucks, Hb Schlegel, Ge Scuseria, Ma Robb, Jr Cheeseman, G. Scalmani, V. Barone, B. Mennucci, Ga Petersson Et Al., Gaussian. *Inc., Wallingford CT* **2009**.
41. Zhao, Y.; Truhlar, D. G., Density Functionals with Broad Applicability in Chemistry. *Acc. Chem. Res.* **2008**, *41*, 157-167.
42. Hehre, W. J.; Ditchfield, R.; Pople, J. A., Self—Consistent Molecular Orbital Methods. Xii. Further Extensions of Gaussian—Type Basis Sets for Use in Molecular Orbital Studies of Organic Molecules. *J. Chem. Phys.* **1972**, *56*, 2257-2261.
43. Hariharan, P. C.; Pople, J. A., The Influence of Polarization Functions on Molecular Orbital Hydrogenation Energies. *Theoretical Chemistry Accounts: Theory, Computation, and Modeling (Theoretica Chimica Acta)* **1973**, *28*, 213-222.
44. Spitznagel, G. W.; Clark, T.; Chandrasekhar, J.; Schleyer, P. V. R., Stabilization of Methyl Anions by First-Row Substituents. The Superiority of Diffuse Function-Augmented Basis Sets for Anion Calculations. *J. Comput. Chem.* **1982**, *3*, 363-371.
45. Clark, T.; Chandrasekhar, J.; Spitznagel, G. W.; Schleyer, P. V. R., Efficient Diffuse Function-Augmented Basis Sets for Anion Calculations. Iii. The 3-21+ G Basis Set for First-Row Elements, Li–F. *J. Comput. Chem.* **1983**, *4*, 294-301.
46. Chiodo, S.; Russo, N.; Sicilia, E., Lanl2dz Basis Sets Recontracted in the Framework of Density Functional Theory. *J. Chem. Phys.* **2006**, *125*, 104107.
47. Lu, T.; Chen, F., Multiwfn: A Multifunctional Wavefunction Analyzer. *J. Comput. Chem.* **2012**, *33*, 580-592.
48. Geerlings, P.; De Proft, F.; Langenaeker, W., Conceptual Density Functional Theory. *Chem. Rev.* **2003**, *103*, 1793-1874.
49. Johnson, E. R.; Keinan, S.; Mori-Sánchez, P.; Contreras-García, J.; Cohen, A. J.; Yang, W., Revealing Noncovalent Interactions. *J. Am. Chem. Soc.* **2010**, *132*, 6498-6506.
50. Reed, A. E.; Curtiss, L. A.; Weinhold, F., Intermolecular Interactions from a Natural Bond Orbital, Donor-Acceptor Viewpoint. *Chem. Rev.* **1988**, *88*, 899-926.
51. Chien, J. C. W., Kinetics of Ethylene Polymerization Catalyzed by Bis-(Cyclopentadienyl)-Titanium Dichloride-

Dimethylaluminum Chloride1. *J. Am. Chem. Soc.* **1959**, *81*, 86-92.
52. Chien, J. C. W.; Wang, B.-P., Metallocene-Methylaluminoxane Catalysts for Olefin Polymerization. V. Comparison of Cp2zrcl2 and Cpzrcl3. *J. Polym. Sci., Part A: Polym. Chem.* **1990**, *28*, 15-38.
53. Chien, J. C. W.; Tsai, W. M.; Rausch, M. D., Isospecific Polymerization of Propylene Catalyzed by Rac-Ethylenebis(Indenyl)Methylzirconium Cation. *J. Am. Chem. Soc.* **1991**, *113*, 8570-8571.

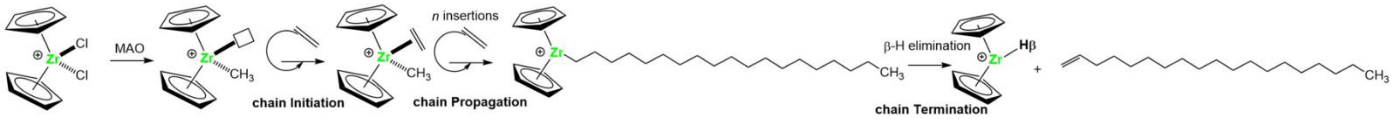
MAO
chain Initiation
n insertions
chain Propagation
β-H elimination
chain Termination

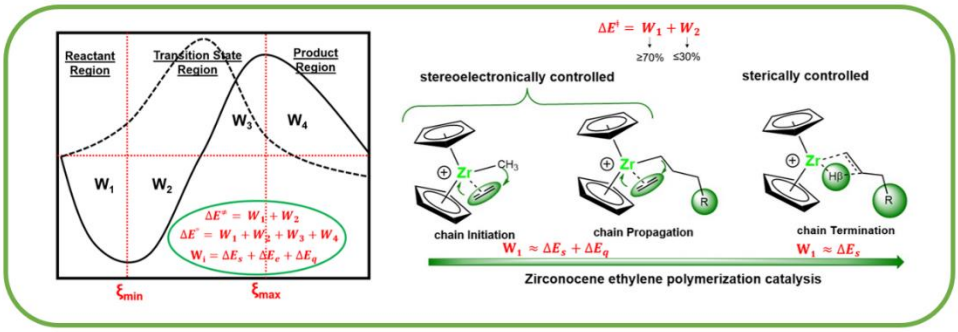
Reactant Region
Transition State Region
Product Region
W1
W2
W3
W4
ξmin
ξmax
stereoelectronically controlled
sterically controlled
chain Initiation
chain Propagation
chain Termination
Zirconocene ethylene polymerization catalysis